SUPPORTING INFORMATION

The Incident Angle Dependence of CHD_3 Dissociation on the Stepped Pt(211) Surface

Helen Chadwick[1], Ana Gutiérrez-González[2], Davide Migliorini[1], Rainer D. Beck[2] and Geert-Jan Kroes[1]*

1. Leiden Institute of Chemistry, Gorlaeus Laboratories, Leiden University, P.O. Box 9502, 2300 RA Leiden, The Netherlands.

2. Laboratoire de Chimie Physique Moléculaire, Ecole Polytechnique Fédérale de Lausanne, CH-1015 Lausanne, Switzerland.

*h.j.chadwick@lic.leidenuniv.nl

S1. Determination of the experimental velocity distribution

The AIMD calculations initially sample a flux weighted velocity distribution, given by[1]

$$f(v)dv \propto v^3 \exp\left(-\left(\frac{v - v_0}{\alpha}\right)^2\right) dv \tag{S1}$$

where v is the velocity, v_0 the stream velocity and α the width of the velocity distribution. The parameters v_0 and α are determined experimentally by using a fast chopper wheel in conjunction with an on axis quadrupole mass spectrometer (QMS) to measure a time of flight (TOF) distribution (t_{TOF}) of the molecular beam. As the QMS measures the density weighted time of flight distribution instead of a flux weighted velocity distribution, v_0 and α can be found using[1]

$$g(t_{\mathrm{neut}})dt \propto \frac{1}{{t_{\mathrm{neut}}}^4} \exp\left(-\left(\frac{\frac{d_{\mathrm{neut}}}{t_{\mathrm{neut}}} - v_0}{\alpha}\right)^2\right) dt \tag{S2a}$$

$$\propto \frac{1}{{t_{\mathrm{neut}}}^4} \exp\left(-\left(\frac{\frac{d_{\mathrm{neut}}}{t_{\mathrm{neut}}} - \frac{d_{\mathrm{neut}}}{t_0^{\mathrm{neut}}}}{\alpha}\right)^2\right) dt \tag{S2b}$$

where t_{neut} is the time taken for the molecules to travel from the chopper to the ionization region of the QMS, which is a distance d_{neut} and t_0^{neut} is the time associated with v_0 i.e. $v_0 = d_{\mathrm{neut}}/t_0^{\mathrm{neut}}$. The measured TOF distributions do not measure t_{neut} directly but instead

$$t_{\mathrm{TOF}} = t_{\mathrm{chop}} + t_{\mathrm{neut}} + t_{\mathrm{ion}} \tag{S3}$$

where t_{chop} accounts for the delay between the $t = 0$ trigger and the molecular beam opening and t_{ion} the time it takes for the ionized molecule to travel a distance d_{ion} through the QMS. Therefore, to be able to obtain v_0 and α from a TOF measurement, a knowledge of d_{neut}, d_{ion} and t_{chop} is required.

t_{chop} arises because the chopper wheel for the TOF measurements has two slits, one of which passes an optocoupler which provides the $t = 0$ trigger for the start of the TOF measurement and the second which allows the molecular beam through. As these two events do not necessarily coincide, this introduces a 'chopper delay' to the measurement. This can be determined by spinning the chopper at different frequencies (f_{chop}) and fitting the t_{TOF} distribution to

$$g(t_{\mathrm{TOF}}) \propto \frac{1}{{t_{\mathrm{TOF}}}^4} \exp\left(-\left(\frac{\frac{1}{t_{\mathrm{TOF}}} - \frac{1}{t_0^{\mathrm{TOF}}}}{\beta} \right)^2 \right) \tag{S4a}$$

$$t_0^{\mathrm{TOF}} = t_{\mathrm{chop}} + t_0^{\mathrm{neut}} + t_{\mathrm{ion}} \tag{S4b}$$

where $\beta (= \alpha / d_{\mathrm{neut}})$ is the width of the distribution. t_0^{TOF} is then plotted against $1/f_{\mathrm{chop}}$, as shown by the example in Figure S1. The chopper delay for a given chopper frequency, $t_{\mathrm{chop}}(f_{\mathrm{chop}})$, can be found using

$$t_{\mathrm{chop}}(f_{\mathrm{chop}}) = t_0^{\mathrm{TOF}}(f_{\mathrm{chop}}) - t_0^{\mathrm{TOF}}(f_{\mathrm{chop}} = \infty) \tag{S5}$$

where $t_0^{\mathrm{TOF}}(f_{\mathrm{chop}} = \infty) = t_0^{\mathrm{neut}} + t_{\mathrm{ion}}$ is the intercept of the plot in Figure S1. Therefore the intercept of the plot should be the same regardless of whether the chopper is spinning clockwise (+ve) or anticlockwise (-ve), which is shown to be the case by the red and black data in Figure S1.

Both t_{neut} and t_{ion} depend on v_0, so the QMS was mounted on a translatable stage to allow v_0 to be determined without prior knowledge of d_{neut} and d_{ion}. TOF distributions were measured at seven different values of d_{neut} for at least three different chopper frequencies and fit using Eqs. (S4) and (S5) to obtain $t_0^{\mathrm{neut}} + t_{\mathrm{ion}}$. As t_{ion} is independent of d_{neut}, the gradient of a plot of Δd_{neut} against $t_0^{\mathrm{neut}} + t_{\mathrm{ion}}$ is equal to v_0. In principle, t_{chop} should also be independent

of d_{neut}, but in practice we found that it did change slightly as the aperture in front of the QMS (which limits the gas flow into the ionization region) also moved as the QMS was moved. This procedure was repeated for several different gas mixes which gave values of v_0 between 550 m/s and 3550 m/s, as shown in Figure S2.

From the knowledge of v_0 and $t_0^{\mathrm{neut}} + t_{\mathrm{ion}}$ a brute force approach was used to find the best value of the parameters d_{neut} and d_{ion} combining Eq. (S2) and the following for t_{ion}

$$t_{\mathrm{ion}} = \frac{d_{\mathrm{ion}}}{\sqrt{{v_0}^2 + \frac{2eU}{M}}} \tag{S6}$$

where e is the electronic charge, U the acceleration voltage of the QMS and M the mass of the ion. To test the values of d_{ion} and d_{neut} obtained from the calibration, the values of v_0 obtained from fitting the TOF distributions at a single d_{neut} using Eqs. (S2), (S3) and (S6) were compared to those obtained by translating the QMS. The results are shown in Figure S3.

For determining the values of v_0 and α experimentally for the AIMD calculations in the main manuscript, the TOF distribution was measured at a single d_{neut} for at least three different f_{chop} and fit using Eqs. (S2), (S3) and (S6) using the values of d_{neut} and d_{ion} determined by the calibration described above. It should be noted that the broadening of the TOF distribution due to the finite size of the chopper slit is also accounted for in the fitting code used. This so-called 'chopper function' was determined with a continuous molecular beam using the on axis QMS used for TOF measurements, which is sensitive to both the direct molecular beam and the scattered gas in the UHV chamber, and an off axis QMS mounted on the side of the machine (the one used for the King and Wells experiments described in the manuscript) which will only detect the scattered component. The signal measured using the on axis and off axis QMSs are shown as red and black lines in Figure S4A respectively. By taking the appropriate weighted difference

between the two, the chopper function can be determined as shown by the red points in Figure S4B. This is compared to the trapezium used to account for the chopper function in the fitting code (blue).

S2. Comparison of different sets of experimental data

Figure S5 presents a comparison of the sticking coefficients obtained for the dissociation of CHD_3 on Pt(211) from the 2016 (red), 2018 A (blue) and 2018 B (black) experiments at normal incidence ($\theta_i = 0°$, $\phi_i = 0°$) before any scaling has been applied to the 2018 A data. As noted in the main paper, the 2018 A data were affected by systematic errors related to there being an unstable backing pressure in the molecular beam expansion during the experiments. This meant that the baseline of the King and Wells measurement when the beam flag was shut was not a straight line (as is the case in Figure 2A) but that it changed during the measurement which introduced an error into the determination of the partial pressure changes which are required to obtain S_0 (see Eq. (1)). As detailed in the manuscript, this problem was resolved and the measurement at E_{trans} = 98.5 kJ/mol repeated (2018 B), which gave a value of S_0 which was approximately 15% smaller than when there was a problem with the backing pressure (2018 A), providing evidence that the unstable backing pressure led to an error when measuring the sticking coefficient. We therefore scaled the 2018 A values of S_0 by the ratio of the 2018 A:2018 B data taken at 98.5 kJ/mol, reducing the values of the 2018 A data by approximately 15%. It should be emphasized that the correction was determined and applied by only considering the set of data (2018 A) and single data point (2018 B) taken in 2018, which is independent of the earlier dataset (2016). The agreement between the 2016 and scaled 2018 A data shown in Figure 3 of the main manuscript demonstrates the validity of the correction made, as agreement between the 2016 and scaled 2018 A data is not a necessary result of the applied correction.

S3. Contribution of trapped trajectories to reaction

Figure S6 presents the sticking coefficients for $\phi_i = 0°$ under laser-off conditions from the 2016 experiments (red), the (scaled) 2018 A experiments (blue), the AIMD calculations (black), and the AIMD calculations where the trajectories that trap have been assumed to react and have been included in the value of S_0 (green). The trapping probability is higher at more grazing angles of incidence, where the component of the energy normal to the Pt(211) plane is smaller.

Our previous work using AIMD calculations with the SRP32-vdW functional failed to reproduce the lower incident energy experimental data (< 75 kJ/mol) with chemical accuracy for laser-off CHD_3 dissociation on Pt(211) at normal incidence[2], where significant trapping probabilities were also seen. In the current work, the normal incidence energy is < 75 kJ/mol for $|\theta_i| > 30°$, where the SRP32-vdW functional still reproduces the experimental sticking coefficients within error bars. This suggests that, for an incidence energy of 96.8 kJ/mol, no contribution from the trapped trajectories to reaction is required to reproduce the experimental S_0 measured for off normal incidence, even though the trapping probability may be high in the AIMD calculations for specific incidence angles.

S4. Pt(211) as a Pt[3(111)×(100)] surface

Previous work by Gee *et al.* has shown that the angle of incidence dependence of methane[3], hydrogen[4] and oxygen[5] dissociation on Pt(533) can be accounted for by considering the four atom wide (111) terraces and one atom high (100) steps on the (533) surface independently. Here, we follow their analysis to see if it also describes the sticking coefficients from the AIMD calculations for $\phi_i = 0°$ under laser-off conditions for CHD_3 dissociation on Pt(211).

Assuming that the (111) terrace and the (100) step can be treated as two independent surfaces[3–5], the angle dependence of the sticking coefficient can be written as[3]

$$S_0(\theta_i) = A^{111}S_0^{111}(0°)\cos^{n^{111}}(\theta_i - \theta_\perp^{111}) + A^{100}S_0^{100}(0°)\cos^{n^{100}}(\theta_i - \theta_\perp^{100}) \quad \text{(S7)}$$

where A^{111} is the fraction of the surface area covered by the (111) terrace, $S_0^{111}(0°)$ the sticking coefficient determined for the Pt(111) surface at normal incidence, n^{111} is the power of the cos(θ) term and $\theta_\perp^{111}$ the angle between the Pt(211) normal and the (effective) normal of the Pt(111) plane. The parameters with the 100 superscript are the same, but for the Pt(100) step. To reduce the number of fitting parameters, we note that $A^{111} + A^{100} = 1$ and take the value of $S_0^{111}(0°)$ to be 6%, which has been determined previously using AIMD calculations at an incident energy of 97.4 kJ/mol and surface temperature of 500 K[2]. Previous work has shown that at high incidence energies, changing the surface temperature does not significantly change the sticking coefficient for methane dissociation on Pt(111)[6,7] so this is a reasonable approximation to make here. Initially, we took $\theta_\perp^{111}$ = -20° due to the geometry of the surface and $\theta_\perp^{100}$ = 20° as Gee *et al.* found the effective normal for the (100) step on the Pt(533) surface to be half way between the Pt(533) normal and the Pt(100) normal[3]. The fit to the data that we obtain using these assumptions (Method A) in Eq. (S7) is shown as an orange line in Figure S7A and the parameters for the fit are given in Table S1. For Pt(211) we find n^{111} = 7.6 and n^{100} = 3.6 which correspond well to the values of 8 and 4 that Gee *et al.* found for methane dissociation on the Pt(533) surface[3].

To further investigate the applicability of Eq. (S7), we calculated the contribution to the sticking coefficients from the AIMD trajectories for reactions which were considered to occur on the (100) step, shown by the shaded region in Figure S7B, and the (111) terrace. These are shown by the gray and white points in Figure S7A, respectively. We then refit the data using Eq. (S7),

fixing only $S_0^{111}(0°)$ to be 6% and $A^{111} + A^{100} = 1$, whilst also restricting the range of values $\theta_\perp^{100}$ and $\theta_\perp^{111}$ could take based on the position of the maxima of the corresponding sticking coefficient distributions shown in Figure S7A (Method B). The fit obtained by making these assumptions is shown as a black line in Figure S7A and the parameters are given in Table S1. The dashed gray line shows the individual contribution from the (100) step and dashed black line from the (111) terrace. We find that $\theta_\perp^{100}$ = 31.3° and $\theta_\perp^{111}$ = -7.6°. Taking the value of $S_0^{111}(0°)$ = 6% gives A^{100} = 0.41 and $S_0^{100}(0°)$ = 10%. This is consistent with calculations by Jackson *et al*. which have shown the activation barrier for methane dissociation on Pt(100) is lower than the barrier on Pt(111)[8], meaning that the sticking coefficient would be expected to be larger on a Pt(100) surface than a Pt(111) surface. However it is not satisfactory that the fitted $\theta_\perp^{100}$ and $\theta_\perp^{111}$ values from the fit do not correspond to the actual values (approximately 40° and -20°, respectively). This could be due to the position of the transition state on the Pt(211) surface, which is on the top site of the step edge atom[2] where we divided the surface into the (111) terrace and (100) step, which is not equivalent to the position of the top site on either the Pt(111) or Pt(100) facet, where the transition states occur on the extended surfaces[8]. Also, the activation barrier for the dissociation of methane on the (111) terrace of Pt(211) is higher than on an extended Pt(111) surface[9], so scaling the value of $S_0^{111}(0°)$ by the area of the (111) terrace on Pt(211) would be expected to overestimate the contribution to the reactivity from the (111) terrace. Whilst the simple model in Eq. (S7) gives a qualitative description of $S_0(\theta_i)$ for CHD_3 dissociation on Pt(211), it is unlikely to be an accurate quantitative description due to the position of the transition state on the surface and the difference in activation barriers[9]. As discussed in the main manuscript, this correlates with the generalized co-ordination numbers of each of the atoms in the Pt(211) surface[10,11].

References

(1) Scoles, G. *Atomic and Molecular Beam Methods*; Oxford University Press: New York, 1988.

(2) Migliorini, D.; Chadwick, H.; Nattino, F.; Gutiérrez-González, A.; Dombrowski, E.; High, E. A.; Guo, H.; Utz, A. L.; Jackson, B.; Beck, R. D.; et al. Surface Reaction Barriometry: Methane Dissociation on Flat and Stepped Transition Metal Surfaces. *J. Phys. Chem. Lett.* **2017**, *8*, 4177–4182.

(3) Gee, A. T.; Hayden, B. E.; Mormiche, C.; Kleyn, A. W.; Riedmüller, B. The Dynamics of the Dissociative Adsorption of Methane on Pt(533). *J. Chem. Phys.* **2003**, *118*, 3334–3341.

(4) Gee, A. T.; Hayden, B. E.; Mormiche, C.; Nunney, T. S. The Role of Steps in the Dynamics of Hydrogen Dissociation on Pt(533). *J. Chem. Phys.* **2000**, *112*, 7660–7668.

(5) Gee, A. T.; Hayden, B. E. The Dynamics of O_2 Adsorption on Pt(533): Step Mediated Molecular Chemisorption and Dissociation. *J. Chem. Phys.* **2000**, *113*, 10333–10343.

(6) Chadwick, H.; Gutiérrez-González, A.; Beck, R. D. Quantum State Resolved Molecular Beam Reflectivity Measurements: CH_4 Dissociation on Pt(111). *J. Chem. Phys.* **2016**, *145*, 174707.

(7) Schoofs, G. R.; Arumainayagam, C. R.; McMaster, M. C.; Madix, R. J. Dissociative Chemisorption of Methane on Pt(111). *Surf. Sci.* **1989**, *215*, 1–28.

(8) Nave, S.; Tiwari, A. K.; Jackson, B. Methane Dissociation and Adsorption on Ni(111), Pt(111), Ni(100), Pt(100), and Pt(110)-(1×2): Energetic Study. *J. Chem. Phys.* **2010**, *132*, 054705.

(9) Chadwick, H.; Guo, H.; Gutiérrez-González, A.; Menzel, J. P.; Jackson, B.; Beck, R. D. Methane Dissociation on the Steps and Terraces of Pt(211) Resolved by Quantum State and Impact Site. *J. Chem. Phys.* **2018**, *148*, 014701.

(10) Calle-Vallejo, F.; Martínez, J. I.; García-Lastra, J. M.; Sautet, P.; Loffreda, D. Fast Prediction of Adsorption Properties for Platinum Nanocatalysts with Generalized Coordination Numbers. *Angew. Chemie Int. Edit.* **2014**, *53*, 8316–8319.

(11) Calle-Vallejo, F.; Tymoczko, J.; Colic, V.; Vu, Q. H.; Pohl, M. D.; Morgenstern, K.; Loffreda, D.; Sautet, P.; Schuhmann, W.; Bandarenka, A. S. Finding Optimal Surface Sites on Heterogeneous Catalysts by Counting Nearest Neighbors. *Science* **2015**, *350*, 185–189.

Table S1. The parameters obtained fitting the $\phi_i = 0°$ laser-off AIMD calculations using Eq. (S7) as described in Section S4. The parameters in bold show the values that were fixed in each fit. In both fits $A^{111} + A^{100} = 1$ was also used.

	A^{111}	$S_0^{111}(0°)$	n^{111}	$\theta_\perp^{111}$ (°)	A^{100}	$S_0^{100}(0°)$	n^{100}	$\theta_\perp^{100}$ (°)
Method A	0.41	**0.06**	7.6	**-20**	0.59	0.10	3.6	**20**
Method B	0.59	**0.06**	6.2	-7.6	0.41	0.10	1.8	31.3

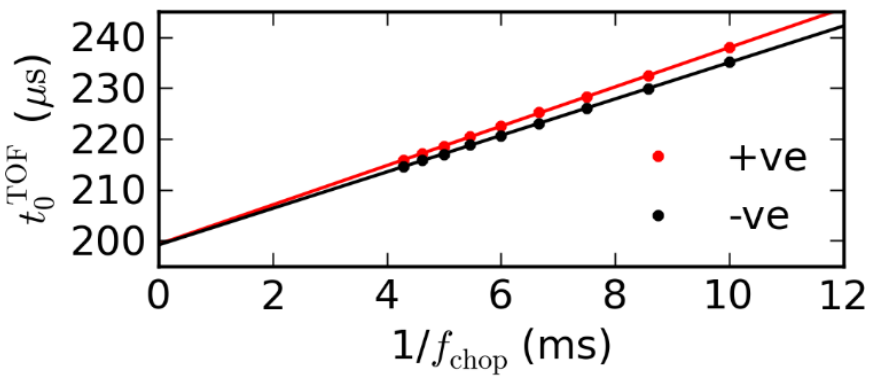

Figure S1. An example of a plot of t_0^{TOF} *vs* $1/f_{\mathrm{chop}}$. See Section S1 for details how t_{chop} can be extracted from this plot.

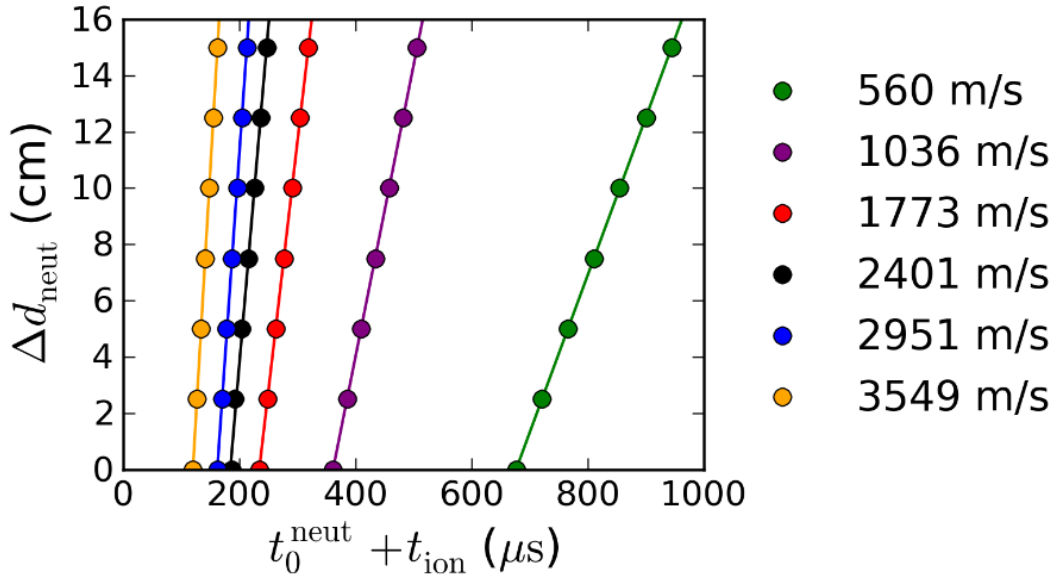

Figure S2. Δd_{neut} *vs* $t_0^{\mathrm{neut}} + t_{\mathrm{ion}}$ obtained by fitting the TOF distributions as described in the main text. The straight lines are fits to the data, the gradients of which give the velocity (which corresponds to v_0) shown in the legend on the right.

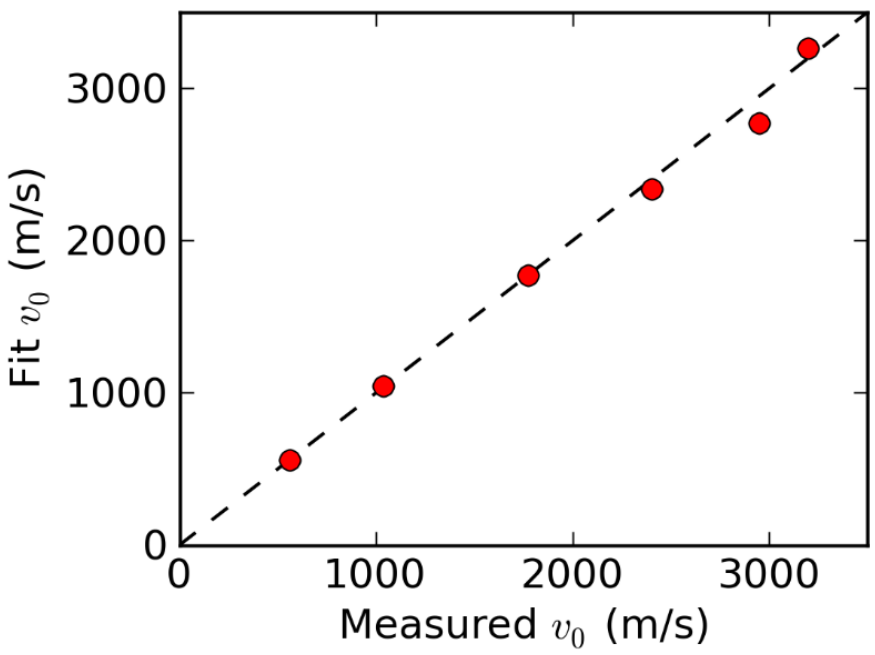

Figure S3. The value of v_0 obtained from a fit to a single time of flight measurement (y-axis) *vs* the value obtained by measuring the time of flight distribution at different values of d_{neut} (x-axis). The dashed line corresponds to y = x.

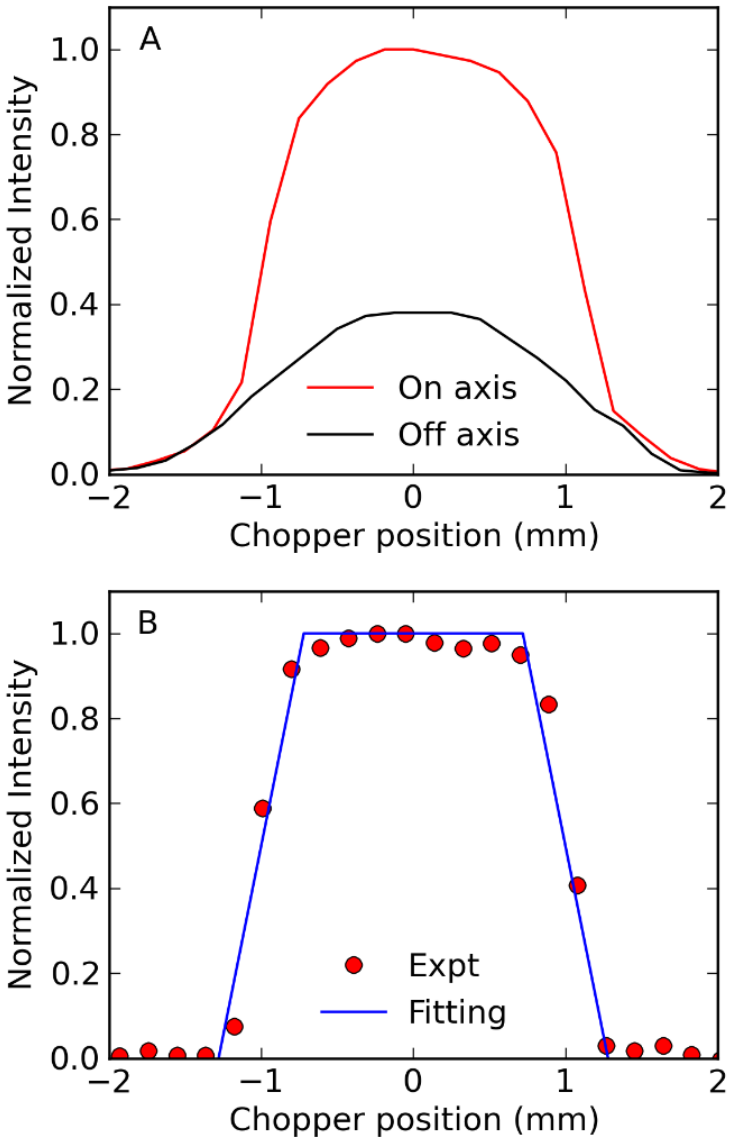

Figure S4. Panel A. The QMS signal measured with the off axis (King and Wells) QMS (black) and on axis (time of flight) QMS (red) as a function of chopper position. The data have been scaled so that the difference produces the chopper function. Panel B. A comparison of the experimentally determined chopper function (red) and the trapezium used in the TOF fitting code to account for the chopper function (blue).

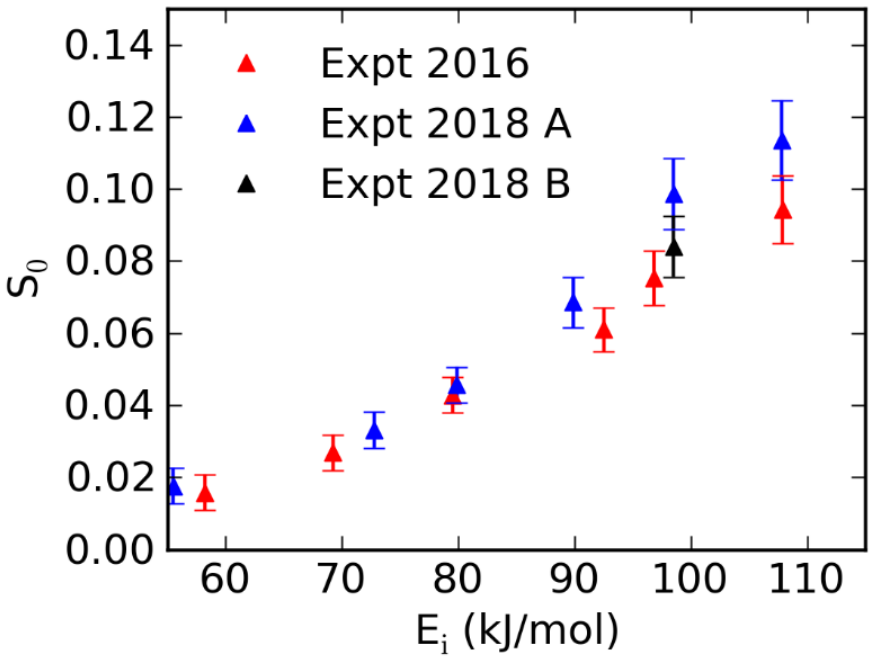

Figure S5. A comparison of the experimental sticking coefficients from three different sets of King and Wells measurements for CHD_3 dissociation on Pt(211) at a surface temperature of 650 K at normal incidence (θ_i = 0°, ϕ_i = 0°).

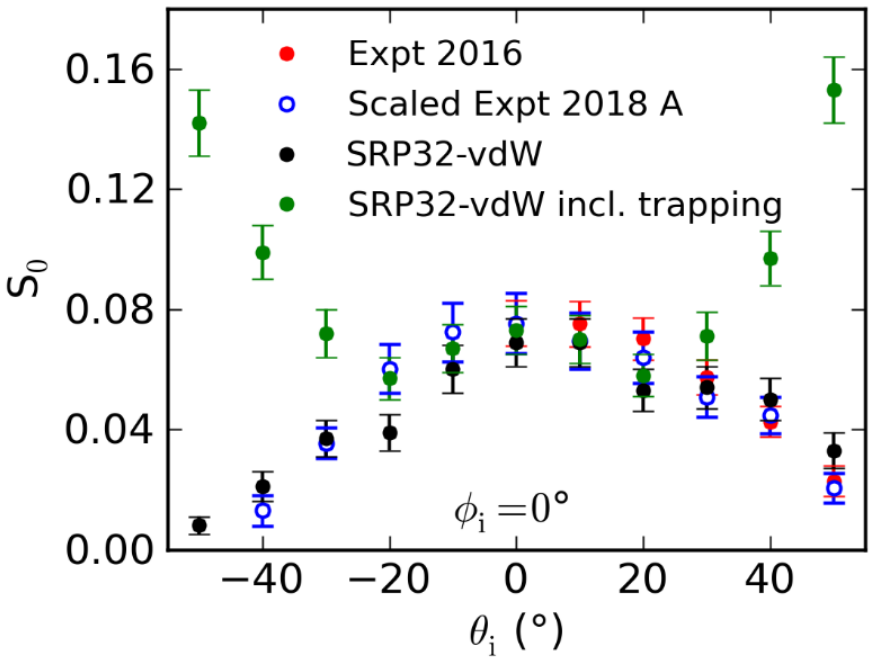

Figure S6. A comparison of the sticking coefficients from the AIMD calculations not including the contribution from trapped trajectories (black circles) and including the contribution from trapped trajectories (green circles) with those from King and Wells experiments at an incident energy of 96.8 kJ/mol (red circles) and scaled sticking coefficients from experiments at an incident energy of 98.5 kJ/mol (blue open circles) for $\phi_i = 0°$.

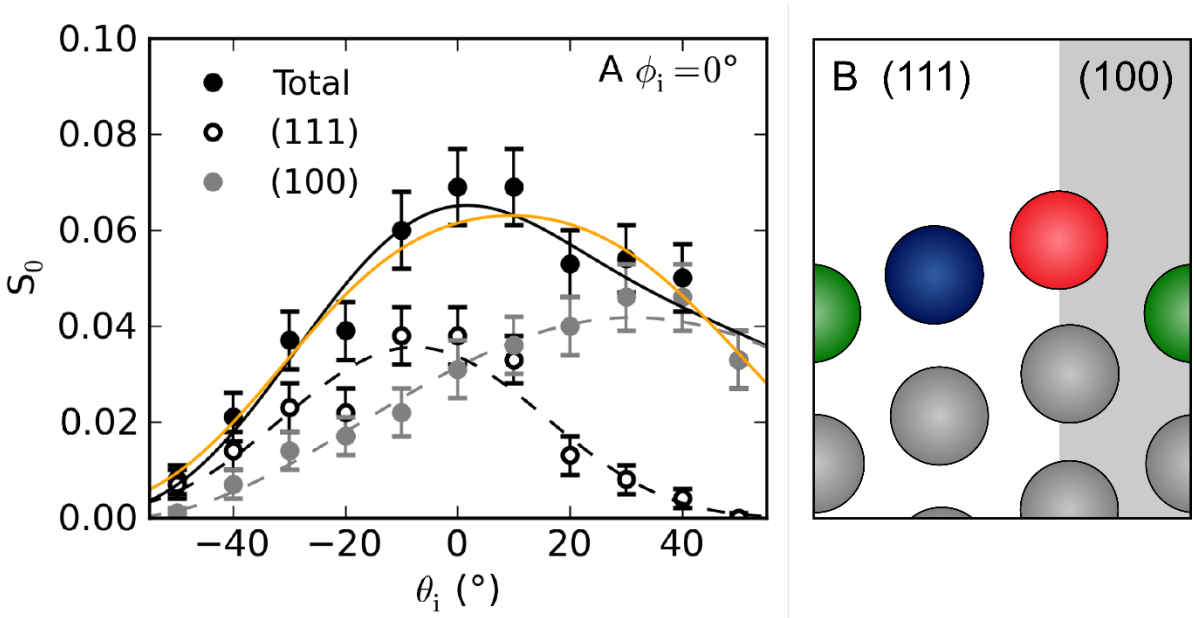

Figure S7. Panel A. Sticking coefficients for the AIMD calculations at ϕ_i = 0° under laser-off conditions (black) and resolved into contributions from the (100) step (gray) and the (111) terrace (white). The orange line is a fit to the data using Eq. (S7), as described by Method A in Section S4, and the dashed lines show the contributions of the reactivity from the (111) terrace (black) and (100) step (gray) to the fit obtained using Eq. (S7) described by Method B (solid black line) in Section S4. Panel B. Schematic of the Pt(211) surface showing the areas of the surface defined as the (100) step (shaded) and the (111) terrace.